Supplementary Material for 'Numerical simulation of bubble dynamics and segregation in binary heptane/dodecane mixtures'†

J. M. Bermudez-Graterol[1]‡, and R. Skoda[1]

[1]Chair of Hydraulic Fluid Machinery, Ruhr University Bochum, Universitätsstr. 150, 44801 Bochum, Germany

S.1. *Pressure evaluation within the liquid*

The liquid pressure p^L is evaluated by Bernoulli's equation and reads

$$p^L = \underbrace{p_w^L + \frac{\left(\rho_m^L\right)^2}{2}\left[\left(u_w^L\right)^2 - \left(u^L\right)^2\right]}_{p^L_{steady}} + \underbrace{\rho_m^L \int_{r=R}^{r} \frac{\partial u^L}{\partial t} dr}_{p^L_{unsteady}} . \tag{S 1}$$

In equation (S 1), p^L consist of a steady contribution p^L_{steady} as well as an unsteady term due to the time derivative of the velocity in terms of $p^L_{unsteady}$. In the unsteady term, the integration is performed from the bubble wall $r = R$ to any location r in the liquid field. By substituting u_w^L and u^L by equations (2.13) and (2.14), we obtain an analytical solution for p^L:

$$\begin{aligned} p^L = & \underbrace{p_w^L + \frac{\left(\rho_m^L\right)^2}{2}\left(1 - \frac{R^4}{r^4}\right)\left(\dot{R} - \frac{\dot{m}''}{\rho^L_{m,w}}\right)^2}_{p^L_{steady}} \\ & + \underbrace{\rho_m^L\left[2\,R\,\dot{R}\left(\dot{R} - \frac{\dot{m}''}{\rho^L_{m,w}}\right) + R^2\left(\ddot{R} - \frac{1}{\rho^L_{m,w}}\frac{d\dot{m}''}{dt}\right)\right]\left(\frac{1}{r} - \frac{1}{R}\right)}_{p^L_{unsteady}} . \end{aligned} \tag{S 2}$$

In the test cases considered, both, the steady and the unsteady term have the same order of magnitude. Therefore, it is important to retain both for the evaluation of p^L. On the other hand, a detailed evaluation of the separate terms of the liquid energy equation (2.10) has revealed that the effect of liquid pressure variation on species diffusion is minor, so that liquid pressure can be omitted in the interdiffusion term. The same holds for its effect on liquid property calculation.

† Journal of Fluid Mechanics (2022), doi:10.1017/jfm.2022.636
‡ Email address for correspondence: Jean.BermudezGraterol@ruhr-uni-bochum.de

S.2. *Mass conservation and species complement for three-species systems*

An exact evaluation of diffusion in multi-species systems is mathematically difficult and costly (Poinsont & Veynante 2005). The introduction of equivalent diffusion coefficients D_α^L (equation (A 17)) and D_α^G (equation (A 22)) is a convenient way to handle diffusion in multi-species systems, but produces two issues: For a three-species system ($N_S = 3$), summing-up equations (2.3) from $\alpha = 1 \cdots N_S$ does generally not fulfil mass conservation in terms of equation (2.2). Moreover, solving equations (2.3) for all three species may violate the species complement equation (2.1). To evaluate this issue, we performed several preliminary tests with different closure variants.

Mass conservation may be ensured by solving equation (2.2) for mixture density. On the other hand, mixture density should fulfil equations of state. Thus gas and liquid mixture density ρ_m^G and ρ_m^L may be evaluated by ideal gas law and mixture rule in terms of equation (2.4) and equation (A 8), respectively, possibly in turn violating equation (2.2). In preliminary tests, we have found that irrespective of how ρ_m^γ is calculated, bubble mass differs by less than 1 %, as the other simulation results presented in § 4 of the main article do. Thus mass conservation is approximately fulfilled, even when ρ_m^γ is obtained by an equation of state instead of equation (2.2).

Mass conservation is exactly fulfilled, if a correction velocity $u_c^\gamma = \sum_{\beta=1}^{N_S} D_\beta^\gamma (\partial y_\beta^\gamma / \partial r)$ is introduced into equation (2.3), according to Poinsont & Veynante (2005):

$$\frac{\partial \left(\rho_m^\gamma y_\alpha^\gamma\right)}{\partial t} + \frac{1}{r^2}\frac{\partial}{\partial r}\left[r^2 \rho_m^\gamma y_\alpha^\gamma \left(u^\gamma + u_c^\gamma\right)\right] = \frac{1}{r^2}\frac{\partial}{\partial r}\left(r^2 \rho_m^\gamma D_\alpha^\gamma \frac{\partial y_\alpha^\gamma}{\partial r}\right) \tag{S 3}$$

It is easily verified that by summing up equations (S 3) over α, equation (2.2) is exactly retained. Consequently, the same kind of correction in terms of $u_{c,w}^\gamma = \sum_{\beta=1}^{N_S} D_{\beta,w}^\gamma \left(\partial y_\beta^\gamma / \partial r\right)\Big|_w$ is introduced in the mass conservation equation (2.22) at the bubble wall:

$$\dot{m}_\alpha''(1 - y_{\alpha,w}^\gamma) - y_{\alpha,w}^\gamma \sum_{\substack{\beta=1 \\ \beta\neq\alpha}}^{N_S} \dot{m}_\beta'' = \rho_{m,w}^\gamma D_{\alpha,w}^\gamma \left.\frac{\partial y_\alpha^\gamma}{\partial r}\right|_w - y_{\alpha,w}^\gamma \rho_{m,w}^\gamma u_{c,w}^\gamma \tag{S 4}$$

By summing up equations (S 4) for $\alpha = 1 \cdots N_S$, 0 is exactly retained on both sides. Thus equations (S 3) and (S 4) fulfil mass conservation, and at the same time mixture density can be obtained by an equation of state (equation (2.4) and equation (A 8)). Equations (S 3) and (S 4) may be solved for only two of three species, and mass fraction of the third species may be obtained by equation (2.1), so that species complement is also fulfilled. Interestingly, regardless of which procedure is preferred, results presented in § 4 of the main article only deviate by less than 1 %. We trace the little effect of mass conservation and species complement back to the relatively fine grid and to the fact that diffusion coefficients are of the same order of magnitude for the three species heptane, dodecane and air. Of course, this finding may not be general but specific to the test cases considered. For convenience, the results presented in § 4 of the main article have been obtained by calculating gas mixture density ρ_m^G by the ideal gas law, equation (2.4), and liquid mixture density ρ_m^L by equation (A 8). We have omitted the correction velocities u_c^γ and $u_{c,w}^\gamma$, and equations (2.3) have been solved for only two of three species. Finally, species complement is fulfilled by solving equation (2.1) for the remaining species.

S.3. *Note on the initialization of fuel mixtures*

Fuel mixtures are specified by their liquid fuel mixing ratio, e.g. a mass fraction of 25 % heptane and 75 % dodecane is referred to as 25/75 % mixture. It should be noted that these

values refer to the pure fuel, which means $y^L_{Hep,0}/y^L_{Fuel,0} = 0.25$ and $y^L_{Dod,0}/y^L_{Fuel,0} = 0.75$, with $y^L_{Fuel,0} = y^L_{Hep,0} + y^L_{Dod,0}$. With regard to the entire liquid mixture including dissolved air, mass fractions slightly deviate from these values. For the initial temperature and pressure of the test case in § 4.1 of the main article, in terms of $T_0 = 293.15\,\mathrm{K}$ and $p^L_{\infty,0} = 10^5\,\mathrm{Pa}$, $y^L_{Fuel,0} = 0.999741$ and $y^L_{Air,0} = 0.000286$. Thus the initial mass fraction in the liquid fuel amounts to $y^L_{Hep,0} = 0.249928$ and $y^L_{Dod,0} = 0.749785$.

It is important to note that this mixture ratio refers to the liquid fuel mixture outside the bubble, while the mixture ratio $y^G_{\alpha,0}$ of the gaseous phase within the bubble results from the equilibrium initialisation. To be more precise, $y^G_{Hep,0}$, $y^G_{Dod,0}$ and $y^G_{Air,0}$ result from equations (A 6) and (A 7).

S.4. *Bubble oscillation after a rapid pressure drop*

S.4.1. *Radial distribution of species within the bubble*

For a 25/75 % heptane/dodecane mixture ratio and for time instants 0 – 5 in figure 2(*b*), radial profiles of y^G_α in the bubble interior are plotted in figure S1 over the dimensionless radial coordinate r/R, where $r/R = 0$ and $r/R = 1$ corresponds to the bubble centre and to the bubble wall, respectively. During bubble expansion at the instants 0 – 3, both vapour components in terms of y^G_{Hep} and y^G_{Dod} show a continuous rise and the same spatial-temporal pattern, while y^G_{Dod} is about two orders of magnitude lower than y^G_{Hep} as already discussed by means of figure 2(*b*). y^G_{Air} shows an opposite trend, which means that bubble content is replenished by vapour due to evaporation at the bubble wall, and at the same time air is diluted. This trend reverses for the compression period instant 4 and instant 5 in the proximity of the bubble wall, which means that the wall values y^G_{Hep} and y^G_{Dod} drop again. The drop of y^G_{Hep} and y^G_{Dod} is confined to the wall proximity and does not reach the bubble centre – note the scale of the abscissa ranging from $r/R = 0.5$ to the bubble wall $r/R = 1.0$. This confinement to the wall proximity is associated with $Pe^G \approx 1$ and means that the diffusion time scale is in the same order as the dynamic time scale. In other words, wall-adjacent effects do reach the bubble centre only after a time delay, because diffusion is too slow that it could completely homogenize the mass fraction field within the bubble. The same holds for the T^G field, which is not shown here for brevity.

S.4.2. *Discrete fuel vs. pseudo-fuel model results*

In figure S2, the fuel distribution is depicted for the discrete fuel as well as the pseudo-fuel model. y^G_{Fuel} and y^L_{Fuel} show a dispensable deviation between both models. The same holds for the radial profiles of other flow variables, e.g. velocity or temperature, which are not shown here for brevity.

S.5. *Bubble growth in superheated water*

Further comparisons to experimental data by Lien (1969) and Board & Duffey (1971) as well as simulation results by Robinson & Judd (2004) are performed. The bubble growth dynamics is presented in figure S3. In accordance with the original presentation of results in Robinson & Judd (2004), a non-dimensionless presentation of results is adopted. The present simulation results show a very good match to literature simulation results for a wide range of pressure and superheat levels which is remarkable, since Robinson & Judd (2004) used a significantly simplified simulation model with omission of air content, interspecies diffusion of water and air, and energy equation within the bubble. A slight overestimation of experiments is within the measurement accuracy (Robinson 2002).

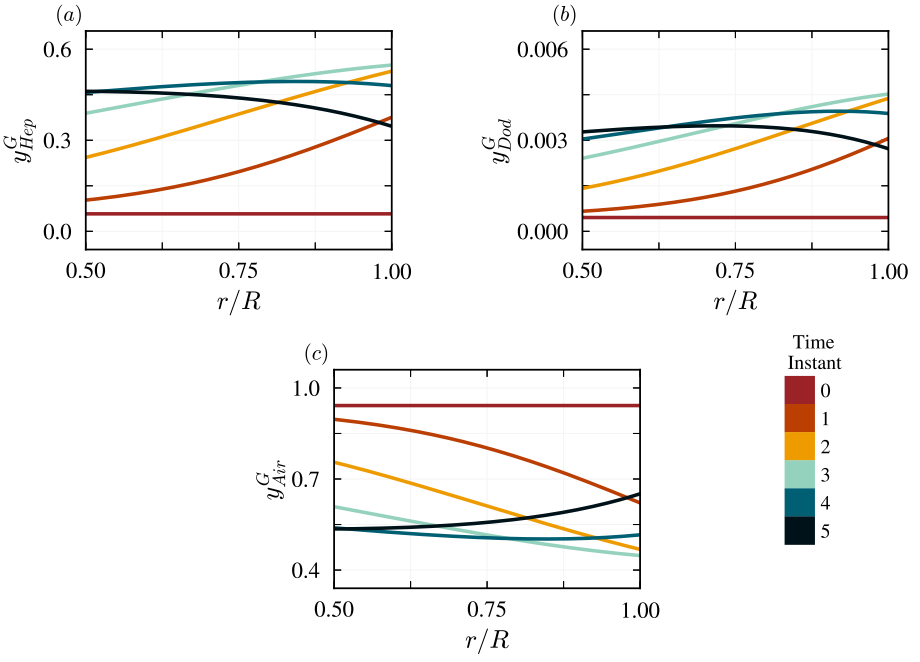

Figure S1: Radial distribution of species inside the bubble for a discrete 25/75 % heptane/dodecane mixture. (*a*) Heptane, (*b*) dodecane and (*c*) air mass fraction within bubble. Time instants 0 – 5 are marked in figure 2(*b*).

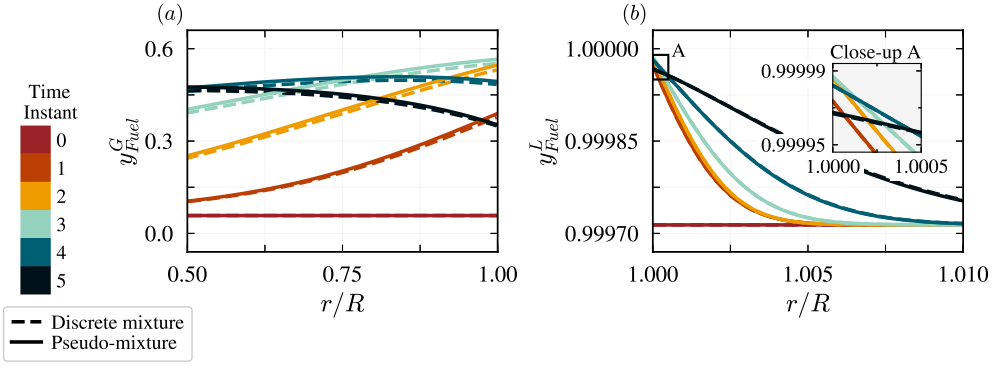

Figure S2: Radial distribution of fuel (*a*) inside and (*b*) around the bubble for a discrete 25/75 % heptane/dodecane fuel mixture and a corresponding pseudo-fuel mixture. Time instants 0 – 5 are marked in figure 2(*b*).

S.6. *Bubble growth in superheated alkane mixtures*

S.6.1. *Time progression of q^L_w and m_{vap}*

The differences between the discrete fuel and the pseudo-fuel model are also reflected in the time progression of heat flux $q^L_w = \lambda^L_{m,w}\ (\partial T^L/\partial r)\big|_w$ on the liquid side of the bubble wall as well as the vapour mass m_{vap} within the bubble which are illustrated in figure S4. The heat flux q^L_w shows a similar pattern as $\dot{R}$. For the pseudo-fuel model, q^L_w is larger than for the discrete fuel model, and converges towards the pure heptane result for any heptane/dodecane

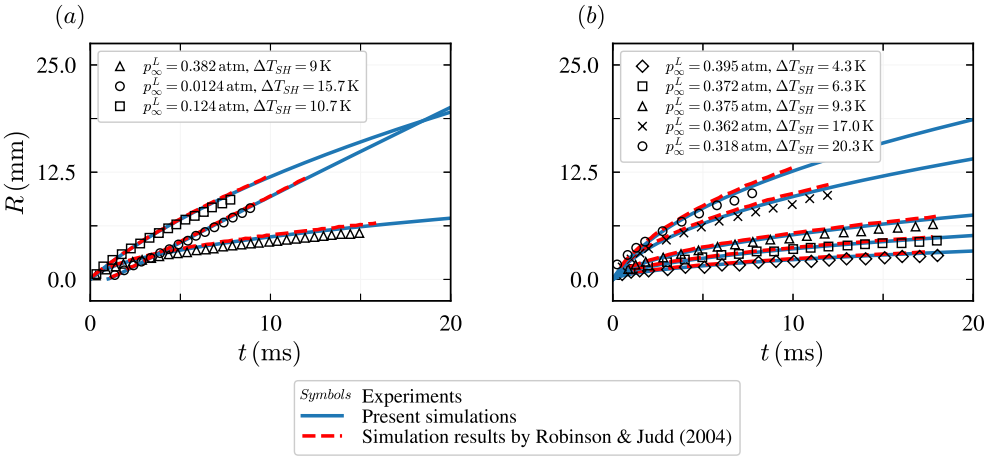

Figure S3: Comparison of present simulation results with experimental measurements of (*a*) Lien (1969) and (*b*) Board & Duffey (1971) as well as with corresponding simulations by Robinson & Judd (2004). Experimental and literature simulation results have been reprinted from Robinson & Judd (2004).

mixture ratio. Also m_{vap} is predicted to be larger by the pseudo-fuel model, particularly for late instants of time.

S.6.2. *Local flow and temperature field in the bubble*

The vapour mass fraction y^G_{Fuel} within the bubble is depicted in figure S5(*a*). The bubble wall is located at $r/R = 1$. The pseudo-mixture distribution temporally precedes the discrete mixture distribution. However, differences are rather small and get somewhat more pronounced for later instants of time. During the later time progression, y^G_{Fuel} approaches the value 1 for both, discrete and pseudo-mixture, which means that the bubble is flooded by fuel vapour, and air mass fraction successively approaches 0. This observation is consistent with the rapid rise of m_{vap}, according to figure S4(*b*).

Profiles of the bubble temperature T^G are illustrated in figure S5(*b*). The liquid and gas wall temperatures are equal according to the thermal equilibrium equation (2.18), and also their gradients are linked by the heat balance equation (2.20). Essentially the entire amount of q^L_w is used for vaporization of the liquid by the latent heat flux $L_m\, \dot{m}''_{Fuel}$, and the heat used for heating or cooling the bubble contents q^G_w is small. For the liquid side gradient $(\partial T^L/\partial r)\big|_w > 0$ holds, as discussed in § 4.2.3 of the main article, figure 9(*b*). This direction of the temperature gradient is continued for the discrete fuel model on the gas side, which means that also $(\partial T^G/\partial r)\big|_w > 0$. For the pseudo-fuel model, on the other hand, a kink of T^G is present at the bubble wall, and from time instant 4 on, $(\partial T^G/\partial r)\big|_w < 0$. This even qualitatively different gas side temperature profiles are directly associated to the separate heat flux terms $q^L_w = \lambda^L_{m,w}\,(\partial T^L/\partial r)\big|_w$ and $q^G_w = \lambda^G_{m,w}\,(\partial T^G/\partial r)\big|_w$ in equation (2.20), as discussed in § 4.2.3 of the main article. The different sign of q^G_w between discrete and pseudo-fuel finally correspond to a fundamentally different radial distribution of T^G.

S.6.3. *Species mass fraction distribution in the bubble*

In figure 8, the radial profiles of species mass fractions in the liquid have been depicted. In the liquid, distinctive boundary layers develop according to figure 8. This result illustration is

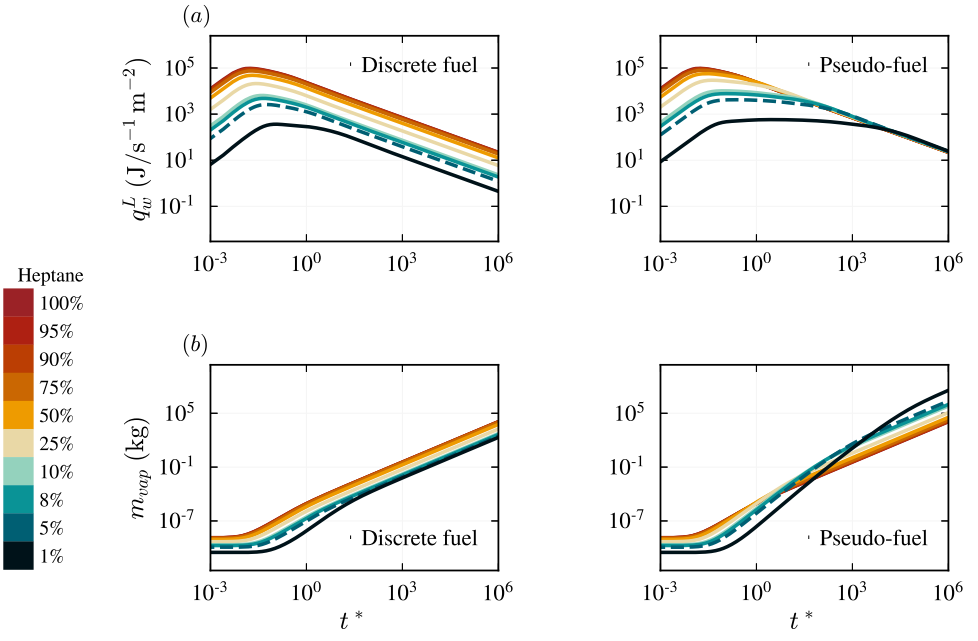

Figure S4: Time progression of (*a*) liquid heat flux q_w^L and (*b*) vapour mass m_{vap} for discrete fuel (left) and pseudo-fuel (right) mixtures in the range 100/0 % to 01/99 % heptane/dodecane mixture ratio. Pure heptane corresponds to the 100/0 % heptane/dodecane mixture. The 05/95 % mixture ratio is marked by a dashed line.

complemented by the gaseous side by figure S6. For the bubble interior, a rather homogeneous distribution of y_{Hep}^G, y_{Dod}^G and y_{Air}^G is present, and thus vapour segregation is moderate.

S.6.4. *Fuel segregation at the bubble wall*

Mass fraction distribution of all three involved species is summarized in figure S7 for several initial mixture ratios in terms of heptane percentage, where the mass fraction of species at the bubble wall is illustrated for $t^* = 10^6$, which is the end of the time range considered. In figures S7(*a*) and S7(*b*), the gaseous and liquid side of the bubble wall is depicted. For clearness of the illustration, both, a linear and a logarithmic scale are presented to the left- and right-hand side, respectively. On the gaseous side, the dominance of heptane within the bubble even for moderate liquid heptane percentage is recognized which has already been discussed in § 4.1 of the main article and can be best discerned on the logarithmic scale in figure S7(*a*),(ii). From another point of view, only for a very low heptane percentage in the liquid, an appreciable dodecane portion within the bubble emerges, which is best seen from the linear scale in figure S7(*a*),(i). Regarding the liquid side, the initial mixture ratio is illustrated by straight dotted lines for the linear scale in figure S7(*b*),(i). Fuel segregation is well discernible by the deviation of the species wall mass fraction from the initial mixture ratio and is most significant for the 50/50 % mixture.

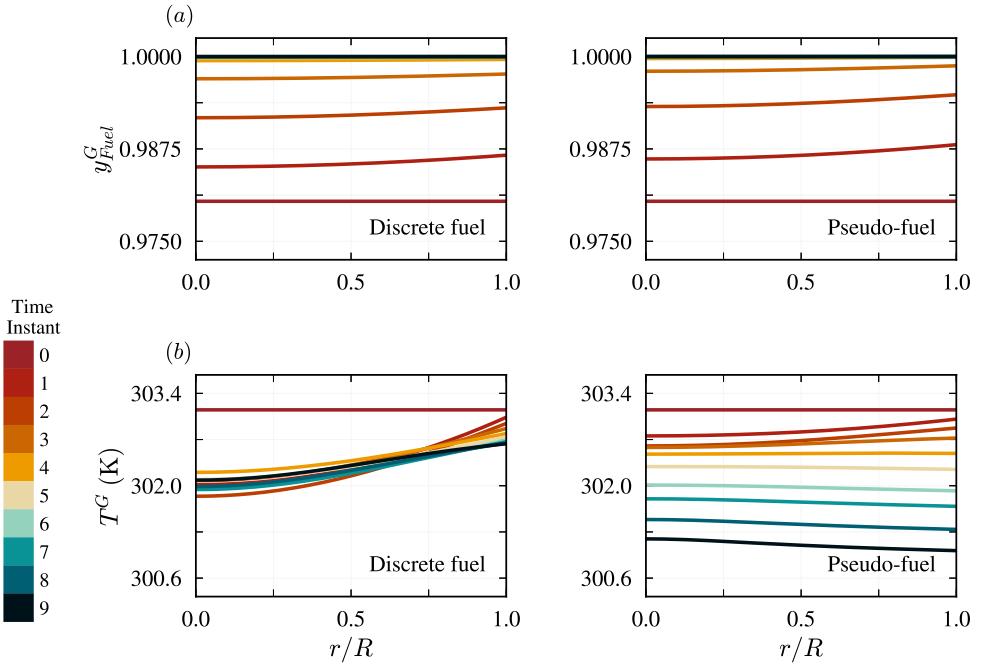

Figure S5: Radial distribution of (*a*) vapour mass fraction and (*b*) bubble temperature for the 05/95 % heptane / dodecane mixture for both, discrete fuel (left) and pseudo-fuel (right).

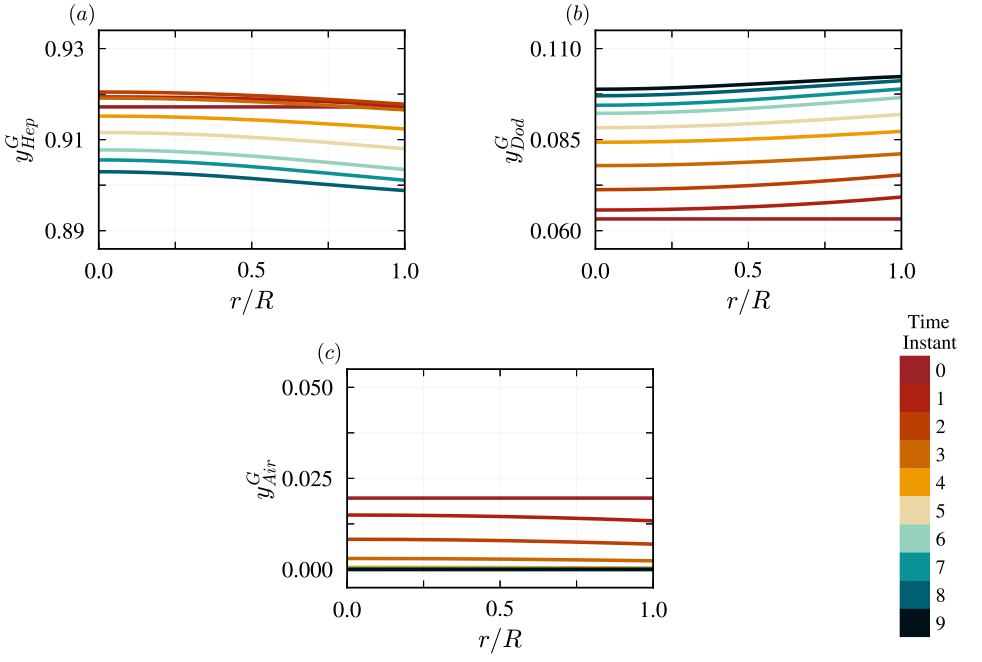

Figure S6: Radial distribution of (*a*) heptan, (*b*) dodecane and (*c*) air mass fraction within the bubble for the discrete 05/95 % heptane/dodecane mixture.

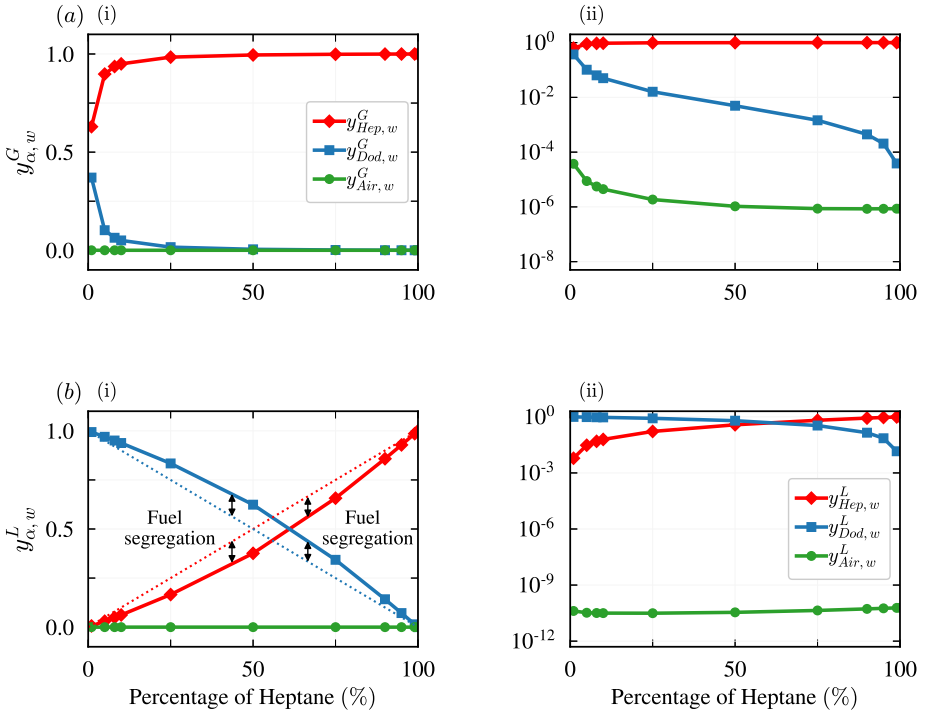

Figure S7: Mass fraction of heptane, dodecane and air at (*a*) gas side and (*b*) liquid side of the bubble wall with (i) linear scale and (ii) logarithmic scale for $t^* = 10^6$ and a discrete fuel mixture variation.

REFERENCES

Board, S.J. & Duffey, R.B. 1971 Spherical vapour bubble growth in superheated liquids. *Chemical Engineering Science* **26** (3), 263–274.

Lien, Y.C. 1969 Bubble growth rates at reduced pressure. Doctoral Thesis, Massachusetts Institute of Technology.

Poinsont, T. & Veynante, D. 2005 *Theoretical and Numerical Combustion*. Edwards.

Robinson, A.J. 2002 Bubble growth dynamics in boiling. Ph.D. Thesis, McMaster University, Hamilton, Ontario, Canada.

Robinson, A.J. & Judd, R.L. 2004 The dynamics of spherical bubble growth. *International Journal of Heat and Mass Transfer* **47** (23), 5101–5113.